RESEARCH ARTICLE

Tailoring turbulence with an active grid

Hakki Ergun Cekli · Willem van de Water

Abstract Using an active grid in a wind tunnel, we generate homogeneous shear turbulence and initiate turbulent boundary layers with adjustable properties. Homogeneous shear turbulence is characterized by a constant gradient of the mean velocity and a constant turbulence intensity. It is the simplest anisotropic turbulent flow thinkable, and it is generated traditionally by equipping a wind tunnel with screens which have a varying transparency and flow straighteners. This is not done easily, and the reachable turbulence levels are modest. We describe a new technique for generating homogeneous shear turbulence using an active grid only. Our active grid consists of a grid of rods with attached vanes which can be rotated by servo motors. We control the grid by prescribing the time-dependent angle of each axis. We tune the vertical transparency profile of the grid by setting appropriate angles of each rod such as to generate a uniform velocity gradient, and set the rods in flapping motion around these angles to tailor the turbulence intensity. The Taylor Reynolds number reached was $R_\lambda = 870$, the shear rate $S = \partial U/\partial y = 9.2 \text{ s}^{-1}$, the nondimensional shear parameter $S^* \equiv Sq^2/\varepsilon = 12$ and $u = 1.4 \text{ ms}^{-1}$. As a further application of this idea we demonstrate the generation of a simulated atmospheric boundary layer in a wind tunnel which has tunable properties. This method offers a great advantage over the traditional one, in which vortex-generating structures need to be placed in the wind tunnel to initiate a fat boundary layer.

H. E. Cekli · W. van de Water (✉)
Physics Department, International Collaboration for Turbulence Research, Eindhoven University of Technology,
P.O. Box 513, 5600 MB Eindhoven, The Netherlands
e-mail: w.v.d.water@tue.nl

1 Introduction

The standard way to stir turbulence in a wind tunnel is by passing the wind through a grid that consists of a regular mesh of bars or rods. In this way, near-homogeneous and near-isotropic turbulence can be made; however, the maximum attainable turbulent Reynolds number is small. Such stirring of turbulence is very well documented. For example, the classic work by Comte-Bellot and Corrsin 1966 concluded that the anisotropy of the velocity fluctuations was smallest for a grid transparency $T = 0.66$. The grid transparency is defined as the ratio of open to total area in a stream-wise projection of the grid. The mesh size M of the grid determines the integral length scale and it typically takes a downstream separation of $40M$ for the flow to become (approximately) homogeneous and isotropic. A relatively new development is the usage of grids with moving elements that can generate homogeneous isotropic turbulence with much larger Reynolds numbers (Makita 1991; Mydlarski and Warhaft 1996). Much more difficult is the generation of tailored turbulent flows, such as homogeneous shear turbulence, or turbulence above a (rough) boundary. We will now briefly review existing techniques to generate these two turbulent flows.

1.1 Homogeneous shear turbulence

Homogeneous shear turbulence is characterized by a constant gradient of the mean velocity dU/dy, but a constant turbulence intensity $u = \langle u^2(y, t) \rangle^{1/2}$, where the average $\langle\ \rangle$ is done over time. Traditionally, shear turbulence is generated (far from walls) using progressive solidity screens that create layers with different mean velocities, combined with means of increasing the turbulence intensity using passive or active grids. Variable solidity passive grids originate in the

pioneering work done more than 30 years ago by Champagne et al. (1970). A somewhat similar technique was used even earlier by Rose (1966), who ingeniously used a succession of parallel rods of equal thickness at variable separation to create a highly homogeneous shear flow, but with a small Reynolds number. A similar approach was followed in Staicu and van de Water (2003), but with a slightly larger Reynolds number. By starting the creation of the gradient by a flow made strongly turbulent by an active grid, Shen and Warhaft reached Reynolds numbers $R_\lambda \approx 10^3$ (Shen and Warhaft 2000). In these experiments the active grid was followed by a variable transparency mesh and flow straighteners. In contrast, in the present paper we illustrate that with a more advanced grid motion protocol the same result can be obtained with an active grid alone.

Homogeneous shear is the simplest thinkable anisotropic turbulent flow. It was used to answer fundamental questions in turbulence research, for example whether turbulent fluctuations become isotropic again at small enough scales and large enough Reynolds numbers (Ferchi and Tavoularis 2000; Pumir and Shraiman 1995; Shen and Warhaft 2000, 2002; Staicu and van de Water 2003; Warhaft and Shen 2002), and whether a hierarchy of anisotropy exponents exists, each of them tied to a representation of the rotation group (Staicu et al. 2003). A recent issue in homogeneous shear is its behavior at asymptotic times (Isaza et al. 2009).

1.2 Simulating the atmospheric boundary layer

Creating a scaled copy of an atmospheric turbulent boundary layer in a wind tunnel is of crucial importance for studying in the laboratory the dispersion of pollution in the atmosphere, or the influence of wind on the built environment. Another timely application is the interaction between the atmosphere and sea, such as the exchange of greenhouse gases between the ocean and the turbulent boundary layer above it.

All these applications demand the creation of a scaled atmospheric boundary layer which is adapted to the roughness structure of the used model inside it. In order to allow for different types of roughness, be it urban, rural or ocean, the properties of this "simulated" boundary layer should be easily adaptable. A large thickness of the simulated atmospheric turbulent boundary layer is very important, as it can accommodate larger models and allows more accurate measurements of velocity or concentration profiles.

When left to its own devices, a turbulent boundary layer will develop spontaneously over a smooth or rough wall; however, it needs a very long wind tunnel test section to grow to a sizable thickness. Therefore, various techniques are used to artificially fatten the growing boundary layer by using passive or active devices.

Passive devices include grids, barriers, spires, and fences at the beginning of the test section of the wind tunnel. Various types, shapes, and combinations have been suggested. Counihan (1973) proposed a modified version of his earlier system (Counihan 1969) which involves a combination of roughness elements, elliptic shaped wedge vorticity generators and barriers to simulate an urban area boundary layer. He obtained reasonably scaled versions of atmospheric turbulent boundary layers. Cook (1973, 1978) refined this method by using various combinations of passive devices. He analyzed the profiles created by different arrangements of grids, elliptic wedge vorticity generators, castellated walls, toothed walls, wooden blocks and coffee-dispenser cups as vortex generators and roughness devices. A quite successful way to initiate a fat boundary layer with passive elements is through the "spires" described by Irwin (1981). These spires must be adapted to the desired flow profile.

Passive methods to simulate an atmospheric boundary layer in wind tunnels are still widely used in laboratories. Their main drawback is that usually a long test section is necessary to install all the vortex generators, roughness elements, etc. According to Simiu and Scanlan (1986), simulations done with the help of passive devices are not expected to result in favorable flow properties in short tunnels; however, a long test section wind tunnel may not be always available.

Several attempts have been reported to simulate an atmospheric boundary layer with active devices. Teunissen used an array of jets in a combination of barriers and roughness elements (Teunissen 1975). He could achieve reasonably accurate simulations for differing types of terrain. Slumen et al. simulated 1980 rural and urban area boundary layers by injecting air through the floor of their wind tunnel. Combining air injection with roughness elements they could increase the thickness of the boundary layer up to 50 cm, which is approximately twice as thick as the one without air injection.

In this paper we will demonstrate that an active grid alone suffices to both tailor homogeneous shear turbulence and simulate the atmospheric turbulent boundary layer, without the need for additional passive structures. Active grids, such as the one used in our experiment, were pioneered by Makita (1991) and consist of a grid of rods with attached vanes that can be rotated by servo motors. The properties of actively stirred turbulence were further investigated by Mydlarski and Warhaft (1996) and Poorte and Biesheuvel (2002). Active grids are ideally suited to modulate turbulence in space-time and offer the exciting possibility to tailor turbulence properties by a judicious choice of the space-time stirring protocol. In our case, the control of the grid's axes is such that we can prescribe the instantaneous angle of each axis through a computer

Fig. 1 a A photograph of the active grid, it consists of seven vertical and ten horizontal axes whose instantaneous angle can be prescribed. They are driven by water-cooled servo motors. The grid mesh size is $M = 0.1$ m. b Schematic drawing (not to scale) of the experimental arrangement. Measurements of the instantaneous u, v, and w velocity components are done 4.6 m downstream of the grid. At this separation, a regular static grid would produce approximate homogeneous and isotropic turbulence
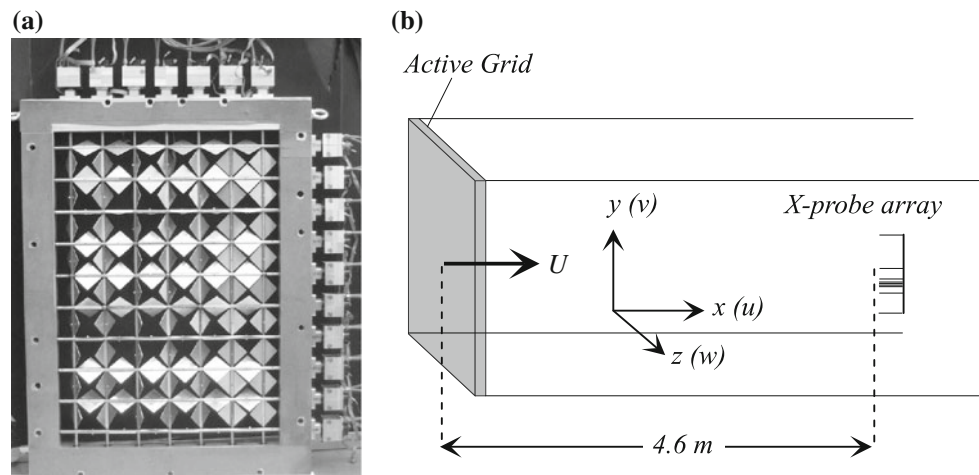
program. To the best of our knowledge, only one other active grid is controlled in a similar way (Knebel and Peinke 2009), other active grids described in the literature do not allow such control and move autonomously in a random fashion. In fact, the random protocols that they use have inspired our operation of the grid, but now the protocol is programmed in software. Our active grid can be used to impose a large variety of patterns, but they are subject to the constraint that a single axis drives an entire row or column of vanes.

The initial position of each rod can be set individually, and each rod can be rotated at a specified speed and direction. These motion parameters can be given as constants prior to the experiment to achieve a periodic modulation, or they can be updated to obtain a more complex modulation e.g. random modulation. The grid is operated by a personal computer, and the instantaneous angle of each rod is recorded to compute the grid state which can be correlated with the measured instantaneous velocity signal. In Fig. 1a a photograph of the grid is shown, together with a sketch of our experiment geometry.

The precise control of our grid enables us to tailor the turbulent flows described in this article, not by (re)placing grids or blocking structures, but by simply changing the parameters of the computer program that controls the active grid. In this paper we will describe the proof of principle. Of the two tailored turbulent flows considered, especially the properties of the atmospheric turbulent boundary layer has been documented in great detail (Counihan 1975); but many of these details of our simulation will be discussed in a future publication.

2 Experimental setup

The active grid is placed in the 8-m-long experimental section of a recirculating wind tunnel. Turbulent velocity

fluctuations are measured at a distance 4.62 m downstream from the grid using an array of hot-wire anemometers. In our experiments we used straight-wire and/or x-wire probes. Each of the locally manufactured hot wires had a 2.5 μm diameter and a sensitive length of 400 μm, which is comparable to the typical smallest length scale of the flow in our experiments (the measured Kolmogorov scale is $\eta \approx 170$ μm). The wires were operated at constant temperature using computer controlled anemometers that were also developed locally. Each experiment was preceded by a calibration procedure. For the straight-wire probes calibration, the voltage-to-air velocity conversion for each wire was measured using a calibrated nozzle. The x-wire probes were calibrated using the full velocity versus yaw angle approach; a detailed description of this method can be found in Browne et al. (1989) and Tropea et al. (2007). The resulting calibrations were updated regularly during the run to allow for a (small) temperature increase of the air in the wind tunnel. The signals captured by the sensors were sampled simultaneously at 20 kHz, after being low-pass filtered at 10 kHz.

The hot-wire array contains ten x-wire probes and was used for the simultaneous measurement of spectra over an interval of 0.23 m centered vertically in the wind tunnel. The nonuniform spacing of the probes is useful for the measurement of structure functions.

3 Homogeneous shear turbulence

Let us now describe the technique for generating homogeneous shear turbulence using an active grid only. First we tune the vertical transparency profile of the grid by setting appropriate angles of each rod such as to generate a uniform velocity gradient, and set the rods in flapping motion around these angles to tailor the turbulence intensity. The overall grid protocol was determined by trial and
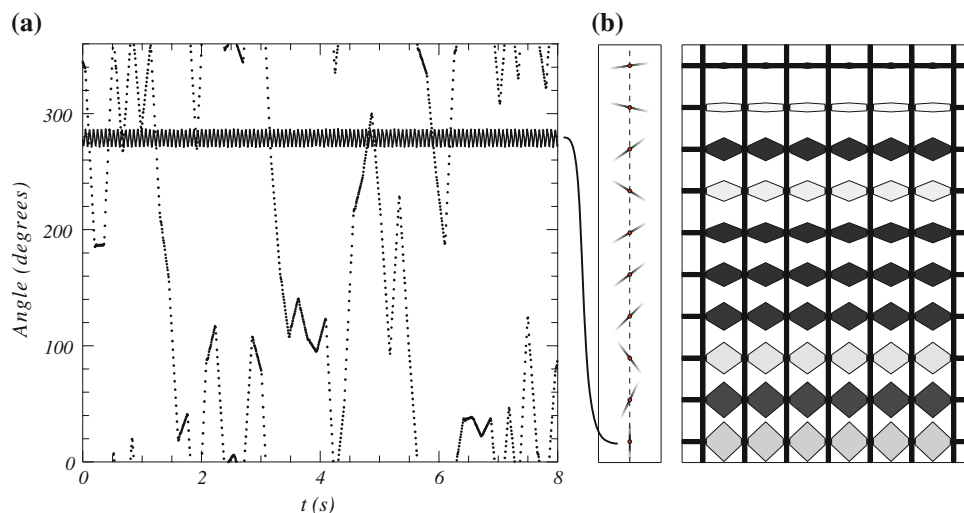
(a)

(b)

Fig. 2 Generation of homogeneous shear turbulence. **a** *Full line*: periodic time-dependent angle of the *lowest horizontal axis* which oscillated around the closed ($3\pi/2$) position, *dots*: random time-dependent angle of a *vertical axis*. **b** The mean angle of the horizontal axes of the grid imposes a variation of the grid transparency that is consistent with a constant gradient of the mean velocity $U(y)$. The vanes with positive angles are painted *black*, those with negative angle are painted *gray*. The mean angles are also illustrated in the *left pane*, with the wind coming from the *left*, each *horizontal rod* oscillates around its mean angle with the same amplitude, but different frequency and relative phase. The *vertical axes* rotate independently randomly over 2π. These random rotations ensure a constant turbulent velocity u

error. In Fig. 2 the pattern of the grid is given which generates homogeneous shear turbulence profile in the wind tunnel. The projections of the rods and horizontal vanes are given, but the vertical vanes are not indicated because they are in a random motion to assure homogeneity of the flow. The vanes connected to the horizontal rods are flapping in a given range and amplitude. The flapping motion of each rod was adjusted independently to maintain a constant turbulence intensity u, and to achieve the desired mean flow gradient.

The mean and fluctuating velocity profile for one wind tunnel mean center flow setting U_c is shown in Fig. 3a. The normalized mean velocity profiles $U(y)/U_c$ for a range of U_c values are shown in Fig. 3b. As it can be seen in this figure, a reasonable homogeneous shear turbulence can be realized in the wind tunnel by assigning proper parameters for each rod of the active grid, without the aid of any additional instrumentation. The Taylor Reynolds number reached was $R_\lambda = 870$, the shear rate $S = \partial U/\partial y = 9.2$ s^{-1}, the nondimensional shear parameter $S^* \equiv Sq^2/\varepsilon = 12$, and $u = 1.4$ ms^{-1}, where $q^2 = 3/2\langle u^2 + v^2 \rangle$ is twice the turbulent kinetic energy, ε is the energy dissipation rate, and u and v are the fluctuating velocities in x and y—direction. Measured profiles at downstream locations $x \in (3.6, 5.6$ m) were not significantly different.

Finally, we show in Fig. 4 the power spectra of the u and w components of the turbulent velocity measured at ten points simultaneously using the probe array. Clearly, not just the turbulent velocity, that is the integral over a spectrum, but also the individual spectra are homogeneous.

At the small scales (large frequencies), the turbulent spectra return to isotropic value $E_{uu}(k_x)/E_{ww}(k_x) = 3/4$. A remaining point of concern is that at very low frequencies, the E_{uu} spectrum does not reach a flat asymptote. Perhaps we still see the direct influence of the moving grid.

Well-documented shear turbulence was reported by Shen and Warhaft (2000) who used an active grid with limited control over the random motion of the axes, together with screen and flow straighteners. As can be judged from a comparison from their Fig. 3 and our Fig. 3, the homogeneity driven by a smart active grid alone is the same as that reported in Shen and Warhaft (2000).

4 Simulation of the atmospheric turbulent boundary layer

In the inner part of the atmospheric turbulent boundary layer, the mean velocity profile can be described by a version of the well-known law of the wall

$$U(y) = \frac{u_*}{\kappa} \ln\left(\frac{y - d}{z_0}\right), \tag{1}$$

where u_* is the friction velocity, κ is the von Kármán constant ($\kappa = 0.41$), z_0 is the roughness height, and where d is the zero-plane displacement, i.e. the effective height of momentum extraction (Castro 2007); it should be placed somewhere within the roughness elements.

In studies of atmospheric turbulent boundary layer simulation, it is customary to represent the mean velocity
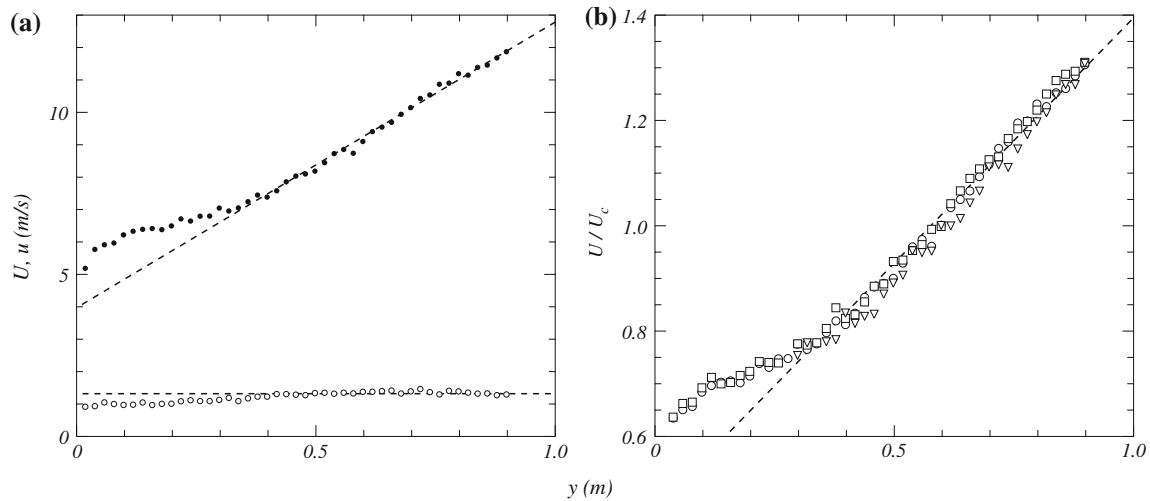
Fig. 3 **a** *Closed dots*: mean velocity profile $U(y)$, it has an approximately constant slope for $y \in (0.3, 0.9\ \mathrm{m})$, corresponding to a shear rate $S = \mathrm{d}U/\mathrm{d}y = 9.2\ \mathrm{s}^{-1}$. *Open circles*: turbulent velocity $u = \langle u(t)^2 \rangle^{1/2}$, it varies 30% over the region $y \in (0.3, 0.9\ \mathrm{m})$ where the turbulence can be considered as homogeneous shear turbulence. **b** Normalized mean velocity profile $U(y)/U_c$, for $U_c = 9.1, 6.1$, and $4.0\ \mathrm{m/s}$, for the *open circles, squares and triangles*, respectively. These velocity profiles were measured at 4.6 m down stream from the active grid. Measured profiles at downstream locations $x \in (3.6, 5.6\ \mathrm{m})$ were not significantly different
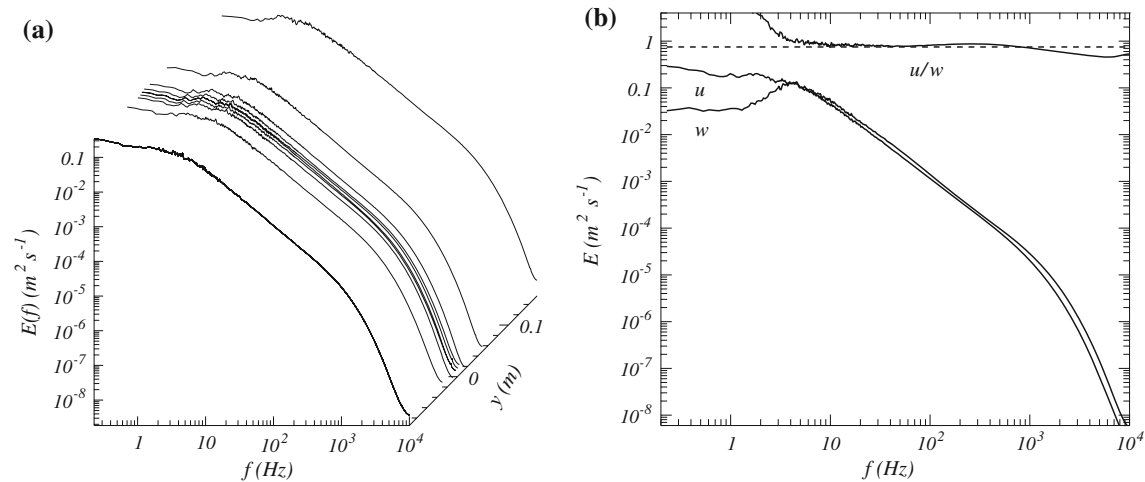

Fig. 4 Energy spectra of homogeneous shear turbulence. **a** Longitudinal spectra $E_{uu}(f)$ measured by the ten probes of the probe array. They illustrate the homogeneity of the flow. The y-coordinate indicates the probe location with respect to the center of the wind tunnel ($y = 0$). **b** Spectra averaged over the probe array. *Full lines* marked by u, w, u/w: E_{uu}, transverse E_{ww}, and E_{uu}/E_{ww}, respectively. *Dashed line*: inertial-range isotropy relation $E_{uu}/E_{ww} = 3/4$

profile over the entire effective height δ of the boundary layer as

$$U(y) = U_\infty \left(\frac{y}{\delta}\right)^\alpha, \tag{2}$$

where the exponent α is $\alpha = 0.1$ for the boundary layer over the ocean, and $\alpha = 0.2, 0.3$ for the boundary layer over a rural and an urban area, respectively. Clearly, while Eq. 2 may provide an approximate and convenient parametrization of the mean velocity profile over a rough wall, it is not compatible with the law of the wall, Eq. 1,

which describes the inner region of the atmospheric turbulent boundary layer.

The art now is to find the proper grid protocol for various types of atmospheric boundary layers. This was done by trial and error. First we tailor the y-dependent grid transparency to the desired boundary layer profile, that is the value of α in Eq. 2. This solidity profile can be realized by selecting the mean angle of the horizontal rods. For two simulated profiles these mean angles are drawn in Fig. 5. We have found that vanes attached to the horizontal axes should point upward toward the incoming flow, which

Fig. 5 Simulated profile of turbulence above a rough boundary above a coastal area (**a**), and above suburban terrain (**c**). **a** *Open circles*: measured profile U/U_∞, with $U_\infty = 9.0$ m/s. *Dashed line*: $U/U_\infty = (y/\delta)^{0.11}$, with δ the boundary layer thickness. **b** Mean angles of the *horizontal axes*, the axes are flapping with a frequency of 3 Hz and an angle amplitude of 7.2° around this mean. **c** *Open circles*: measured profile U/U_∞, with $U_\infty = 11.5$ m/s. *Dashed line*: $U/U_\infty = (y/\delta)^{0.22}$, with δ the boundary layer thickness. **d** Mean angles of the *horizontal axes*, the axes perform flap around these mean angles, frequency 2–3 Hz and amplitude 7.2°–18°. In both cases the boundary layer thickness $\delta = 0.71$ m. Note that the *vertical dimension of the grid is 1 m*, while the profiles are shown for $y \in (0, 0.75 \text{ m})$
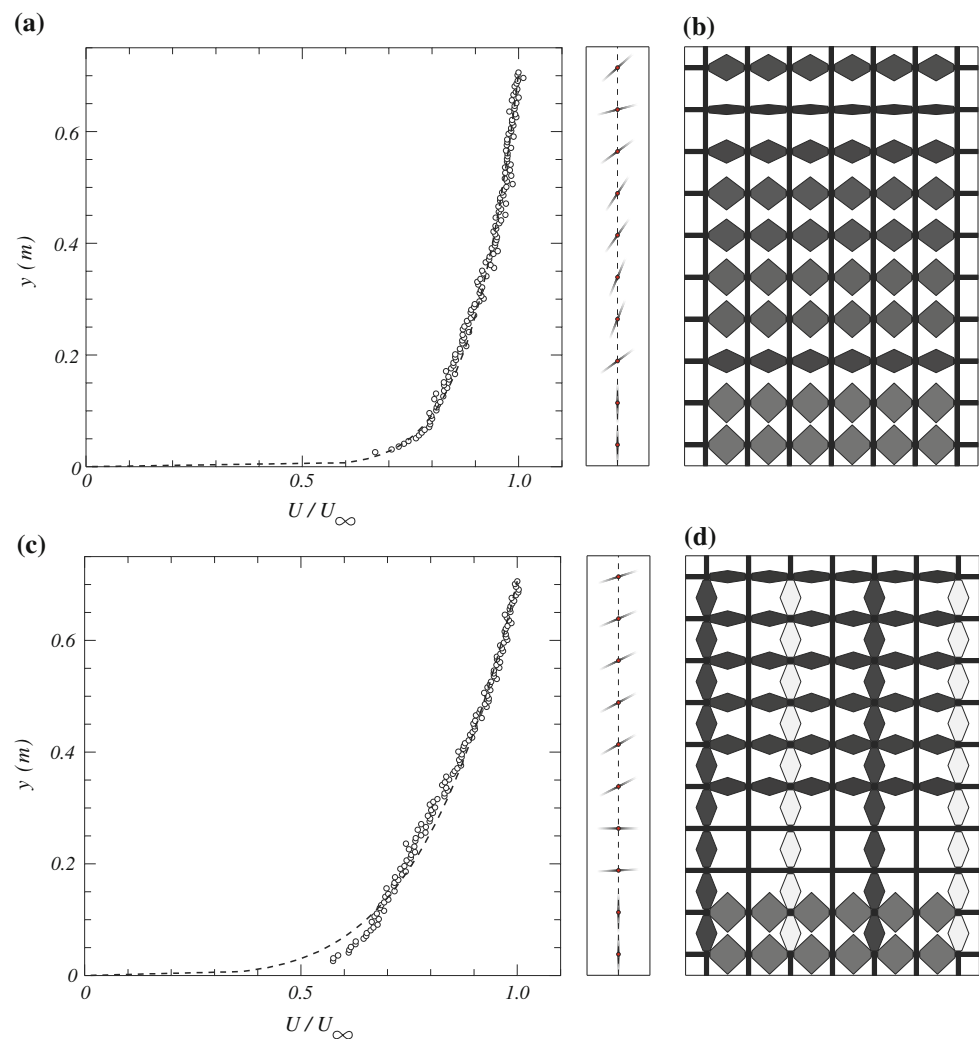
helps to thicken the velocity profile. In some simulations for relatively small α values we use only horizontal rods but for some others we need to use some of vertical rods as well.

In the next step we set the vanes in motion, and change their amplitude and frequency until the desired power-law profile is obtained. The chosen amplitudes and frequencies are also indicated in Fig. 5. This choice is made heuristically, using the following guidelines. To thicken the profile we flap the horizontal rods with a judiciously chosen amplitude and frequency. The amplitude of this flapping motion has a small influence on the mean flow profile, which mainly depends on the mean angle of the rod. We use this influence to fine-tune the profile. The angular amplitude of these periodically flapping axes varies between 9° and 36°, with frequencies between 2 and 3 Hz.

Some of the vertical rods are put in a random motion to assure homogeneity. The used protocol for random motion is to rotate the axis with a randomly chosen rotation rate in one direction, changing to another random rotation

rate after a random time interval. In these experiments, the rotation rates was picked uniformly from the interval $(0, 4 \text{ s}^{-1})$, and the time duration were picked from $(0, 200 \text{ ms})$. The simulated overall mean profile is shown in Fig. 5, while the velocity profile of the inner part of the boundary layer is shown in Fig. 6.

The inner part of the simulated turbulent boundary layer is shown in Fig. 6a. Below $y = 0.1$ m, a logarithmic mean velocity profile $U(y)$ is observed. Its parameters u_*, d, and z_0, were determined by a fit of Eq. 1 to the measured profile. Briefly, $U(y)$ is plotted as a function of $\ln(y - d)$ and the displacement length d was selected which provided a linear dependence over the largest range of y. The shear velocity u_* then follows from the slope of this line, while z_0 is the intercept of this line with the horizontal axis. However, as the closest separations of our probe to the boundary was not smaller than $y = 1$ cm, these parameters could not be determined accurately. The measured Reynolds stresses over the entire boundary are shown in Fig. 6b. A point of concern is that the shear stress $\langle -uv \rangle$, where u and v are the
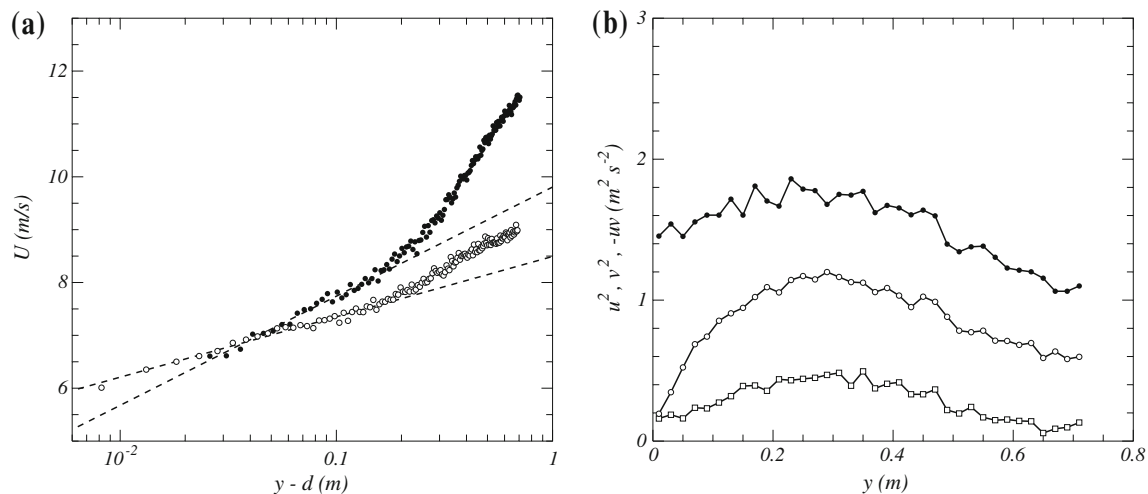
Fig. 6 a *Open circles*: simulated mean velocity profile $U_{\alpha=0.11}(y)$ above a coastal area, *closed dots* $U_{\alpha=0.22}$ above suburban terrain. *Dashed lines* fits with: $U_{\alpha=0.11}(y) = (u_*/\kappa)\ln((y-d)/z_0)$, with $u_* = 0.21$ m/s, $d = 0.018$ m, and roughness length $z_0 \approx 3 \times 10^{-7}$ m, and

$U_{\alpha=0.22}(y) = (u_*/\kappa)\ln((y-d)/z_0)$, with $u_* = 0.41$ m/s, $d = 0$, and $z_0 \approx 5 \times 10^{-5}$ m. **b** Reynolds stresses for the profile with $\alpha = 0.22$, $\langle u^2 \rangle$, $\langle v^2 \rangle$, and $\langle -uv \rangle$, *dots*, *open circles and open squares*, respectively

fluctuating velocities in x and y—direction, is much larger than u_*^2 as derived from the fit of Eq. 1. This implies that the inner part of our simulated atmospheric turbulent boundary layer does not conform the turbulent boundary layer over a rough surface. However, without roughness elements after the initiation of the atmospheric turbulent boundary layer with the active grid, our turbulent boundary layer is not expected to be in equilibrium.

5 Conclusions

We have demonstrated how tailored turbulence can be made by programming the motion of an active grid, with no recourse to passive flow structuring elements. This worked best for homogeneous shear turbulence, where the results are comparable to those obtained earlier with the help of additional passive devices. The initiation of a simulated atmospheric turbulent boundary layer was presented as a proof of principle; our setup lacks roughness elements to maintain the turbulent boundary layer. Also, we have not yet exhausted the possibilities of the active grid; especially the simulation of the atmospheric turbulent boundary layer could be improved by adding extra vanes.

Selecting the grid parameters by hand, guided by simple rules, such as tailoring the mean profile through the solidity set by the average vane angle and then tuning the turbulence intensity by flapping the vane randomly around this mean angle, is only a first step. One could readily envisage automated procedures borrowed from the active field of turbulence control. While in this field the goal is to prevent turbulence or diminish turbulent drag, our goal would be to shape and possibly enhance turbulence.

References

Browne LWB, Antonia RA, Chua LP (1989) Calibration of X-probes for turbulent flow measurements. Exp Fluids 7:201–208

Castro I (2007) Rough-wall boundary layers: mean flow universality. J Fluid Mech 585:469–485

Champagne FH, Harris VG, Corrsin S (1970) Experiments on nearly homogeneous turbulent shear flow. J Fluid Mech 41:81

Comte-Bellot G, Corrsin S (1966) The use of a contraction to improve to isotropy of grid-generated turbulence. J Fluid Mech 25:657–682

Cook NJ (1973) On simulating the lower third of the urban adiabatic boundary layer in a wind tunnel. Atmos Environ 7:49–71

Cook NJ (1978) Wind-tunnel simulation of the adiabatic atmospheric boundary layer by roughness, barrier and mixing device methods. J Ind Aerodyn 3:157–176

Counihan J (1969) An improved method of simulating an atmospheric boundary layer in a wind tunnel. Atmos Environ 3:197–214

Counihan J (1973) Simulation of an adiabatic urban boundary layer in a wind tunnel. Atmos Environ 7:673–689

Counihan J (1975) Adiabatic atmospheric boundary layers: a review and analysis of data from the period 1880–1972. Atmos Environ 9:871–905

Ferchi M, Tavoularis S (2000) Reynolds number effects on the fine structure of uniformly sheared turbulence. Phys Fluids 12(11): 2942–2953

Irwin NPAH (1981) The design of spires for wind simulation. J Wind Eng Ind Aerodyn 7:361–366

Isaza JC, Warhaft Z, Collins LR (2009) Experimental investigation of the large-scale velocity statistics in homogeneous turbulent shear flow. Phys Fluids 21:065,105

Knebel P, Peinke J (2009) Active grid generated turbulence. In: Eckhardt B (ed) Advances in Turbulence XII, Springer Proceedings in Physics, vol 132, p 903

Makita H (1991) Realization of a large-scale turbulence field in a small wind tunnel. Fluid Dyn Res 8:53–64

Mydlarski L, Warhaft Z (1996) On the onset of high-Reynolds-number grid-generated wind tunnel turbulence. J Fluid Mech 320:331–368

Poorte REG, Biesheuvel A (2002) Experiments on the motion of gas bubbles in turbulence generated by an active grid. J Fluid Mech 461:127–154

Pumir A, Shraiman BI (1995) Persistent small-scale anisotropy in homogeneous shear flows. Phys Rev Lett 75(17):3114–3117

Rose WG (1966) Results of an attempt to generate a homogeneous turbulent shear flow. J Fluid Mech 25:97

Shen X, Warhaft Z (2000) The anisotropy of the small scale structure in high Reynolds number $Re_\lambda \gg 1000$ turbulent shear flow. Phys Fluids 12(11):2976–2989

Shen X, Warhaft Z (2002) Longitudinal and transverse structure functions in sheared and unsheared wind-tunnel turbulence. Phys Fluids 14(1):370–381

Simiu E, Scanlan RH (1986) Wind effects on structures. Wiley, New York

Sluman TJ, van Maanen HRE, Ooms G (1980) Atmospheric boundary layer simulation in a wind tunnel, using air injection. App Sci Res 36:289–307

Staicu A, van de Water W (2003) Small-scale velocity jumps in shear-turbulence. Phys Rev Lett 90:94501–94503

Staicu A, Vorselaars B, van de Water W (2003) Turbulence anisotropy and the SO(3) description. Phys Rev E 68:46,303–4636

Teunissen HW (1975) Simulation of the planetary boundary layer in a multiple-jet wind tunnel. Atmos Environ 9:145–174

Tropea C, Yarin AL, Foos JF (2007) Springer handbook of experimental fluid mechanics. Springer, New York

Warhaft Z, Shen X (2002) Some comments on the small scale structure of turbulence at high Reynolds number. Phys Fluids 13:1532